Proximal and Distal Gut Mucosa Adapt Differently to Westernized Diet, Promoting an Insulin-Resistant Dysmetabolic State

Jason A. West,[1] Anastasia Tsakmaki,[2] Jason H. S. Huang,[1] Soumitra S. Ghosh,[3] David G. Parkes,[4] Pernille Wismann,[5] Kristoffer T. G. Rigbolt,[5] Philip J. Pedersen,[5] Polychronis Pavlidis,[6,7] David Maggs,[1,8] Juan Carlos Lopez-Talavera,[1] Gavin A. Bewick,[2]* Harith Rajagopalan[1]

[1]Fractyl Laboratories Inc, Lexington, MA, 02421, USA

[2]Diabetes Research Group, School of Life Course Sciences, Faculty of Life Science and Medicine, King's College London, London, WC2R 2LS, England, UK

[3]Doon Associates, San Diego, CA, 92129, USA

[4]DGP Scientific Inc, San Diego, CA, 92014, USA

[5]Gubra ApS, Hørsholm Kongevej 11B, Hørsholm, DK-2970, Denmark

[6]Centre for Inflammation Biology and Cancer Immunology, King's College London, London, WC2R 2LS, England, UK

[7]Department of Gastroenterology, Guy's and St. Thomas' NHS Foundation Trust, London, SE1 9RT, UK

[8]Present address: Becton Dickinson Technologies & Innovation, Raleigh-Durham, NC, 27709, USA

*Correspondence: Gavin A Bewick, PhD, Diabetes Research Group, Guys Campus King's College London, London SE1 1UL, UK Phone: +44 (0)20 7836 6274, gavin.bewick@kcl.ac.uk

Character Count: 53973

Financial Support: Provided by Fractyl Laboratories Inc.

SUMMARY

The intestine adapts to local nutrient exposure, but little is known about the effect of high-fat diets (HFDs) on topographically distinct segments of the gut. Here, we show obesogenic diets induce different effects on proximal versus distal intestinal mucosa *in vivo* and mouse and human organoid models. Notably, we demonstrate proximal gut hyperplasia and distal gut hypoplasia in response to HFD in rodents and show that surgical and pharmacologic interventions that circumvent this altered mucosal physiology improve glucose metabolism. In addition, organoids derived from the duodenum of mice or humans demonstrate increased stemness (self-renewal and differentiation) and growth response to increasing amounts of lipid or glucose, while ileal organoids displayed a functionally different and often opposite growth response profile. These results highlight the important role of the small intestinal mucosa in regulating metabolic homeostasis in health and disease and open new avenues and therapeutic approaches to treat metabolic diseases.

Summary Word Count: 149

Key Words: duodenum, duodenal diseases, intestinal mucosa, metabolic diseases, Western diet

INTRODUCTION

Excessive consumption of diets high in saturated and trans fats and refined sugar is one of the primary drivers of insulin resistance and hyperinsulinemia that underlie the global obesity and metabolic disease epidemics.(Cordain et al., 2005; Danaei et al., 2013) The evidence that gastrointestinal procedures (e.g., bariatric/metabolic surgery) can induce dramatic and long-lasting improvement of type 2 diabetes (T2D) highlights the important but under-recognized role of the gut as a regulator of metabolism in health and disease. In patients with obesity and/or obesity-related disorders, such as T2D and non-alcoholic fatty liver disease, procedures that bypass the upper small intestine (e.g., Roux-en-Y gastric bypass [RYGB] surgery, duodenal-jejunal bypass) elicit weight-independent improvements in glycemic control and insulin resistance.(Ferrannini and Mingrone, 2009; Jacobsen et al., 2012; Jirapinyo et al., 2018; Laursen et al., 2019; Mingrone et al., 2012; Rubino et al., 2006; Salinari et al., 2013; Umeda et al., 2011; Zervos et al., 2010) Understanding the mechanisms by which bypass of the duodenum and/or nutrient delivery to the distal bowel leads to lasting improvements in metabolic homeostasis provides an opportunity to refine current treatments and develop new therapies for metabolic diseases.(Cummings et al., 2007; de Jonge et al., 2013; Sandoval, 2016)

The epithelium of the gastrointestinal tract plays a key role in tuning nutrient sensing, absorption, use, and storage.(Cummings and Overduin, 2007; Rao and Wang, 2010) Consisting broadly of five distinct cell types (enterocytes, Paneth, goblet, tuft, and enteroendocrine cells [EECs]), the gut epithelium renews itself every 3 to 5 days from cycling leucine-rich repeat-containing G-protein-coupled receptor (LGR5)-positive crypt stem cells.(Barker et al., 2007) EECs comprise the largest endocrine system in the body and play a central role in integrating diverse signals from the luminal environment (including nutrients, bile acids, and microbial

metabolites) to regulate metabolic physiology.(Gribble and Reimann, 2019) More than 20 different hormones and neuropeptides are expressed in subsets of terminally differentiated EECs.(Haber et al., 2017) The topographic distribution of hormone production varies along the length of the gut. For example, the incretin hormone glucose-dependent insulinotropic polypeptide (GIP) is expressed by K cells, which are predominately located in the proximal small intestine (duodenum and jejunum), while glucagon-like peptide-1 (GLP-1) is produced by L-cells, which are more abundant in the distal small intestine (ileum) and colon.(Gehart et al., 2019; Reimann and Gribble, 2016) These regional gut hormones are key regulators of glucose homeostasis and have become targets for the development of metabolic-associated therapies. GIP is positively associated with T2D and insulin resistance,(Theodorakis et al., 2004) and inhibition of GIP signaling in animal models has been shown to prevent obesity and insulin resistance induced from a high-fat diet (HFD).(Althage et al., 2008; Killion et al., 2018; Miyawaki et al., 2002) In contrast, GLP-1 is used therapeutically to improve glycemic control via an enhanced insulin response to glucose and other mechanisms. GLP-1 insufficiency has been reported in patients with T2D and insulin resistance,(Nauck et al., 2011) while post-prandial GLP-1 expression dramatically increases after RYGB surgery.(Salehi et al., 2011) Notably, following RYGB and gastric sleeve procedures, GLP-1 secretion increases the more distally nutrients are delivered.

The gut architecture adapts to nutrient exposure over time. Individual segments of the gut respond differently to both acute and chronic nutrient exposure, resulting in acute and chronic alteration of intestinal absorptive and signaling responses. For example, nutrient stimulation produces differential effects on gene expression and mucosal thickness along the length of the gut.(de Wit et al., 2008) Intestinal plasticity may be maladaptive in metabolic disease. In rodent and pig models, HFD causes morphologic and functional changes in the duodenum, including hyperplasia and proliferation of K cells with a corresponding increase in the production and

secretion of GIP.(Adachi et al., 2003; Bailey et al., 1986; Gniuli et al., 2010) In rats, HFD leads to impaired glucose sensing in EECs and enterochromaffin cells. Moreover, in human studies, abnormal mucosal hypertrophy and increases in EEC and enterocyte numbers in the proximal small intestine (including the duodenum) have been reported in diabetic patients compared with non-diabetic controls.(Theodorakis et al., 2006; Verdam et al., 2011) In the duodenum of T2D patients, nutrient-induced signaling exerts an insulin-resisting/glucose-raising effect, while the ileum exerts an insulin-sensitizing/glucose-lowering effect on nutrient exposure in the same patients.(Zhang et al., 2019) Results from studies have also shown that proteins secreted from the jejunum of diabetic (db/db) mice promote insulin resistance when isolated and administered to non-diabetic mice,(Salinari et al., 2013) suggesting that the alterations of intestinal mucosa observed in T2D might be mechanistically linked with the pathophysiology of the disease.

The substantial and growing body of literature points to the intestine as a critical metabolic signaling center and regulator of metabolic homeostasis. Fundamental questions regarding the relative contributions of factors produced by the proximal and distal small intestine—and the potential for a causal role of intestinal mucosal changes in obesity and the dysmetabolic state—remain unanswered. To further characterize nutrient-induced gut adaptation, we examined hormonal and transcriptional changes in the small intestine of high-fat, diet-induced obese (DIO) rodents and the effects of direct stimulation with lipid and glucose on proximal and distal intestinal epithelial growth using rodent and human organoids. To investigate the pathophysiological relevance of nutrient-induced gut adaptation, we studied the effect of surgical intervention (RYGB) on proximal and distal intestinal morphology and gene expression in DIO rodents and tested the effect of pharmacologic manipulation of proximal (GIP) and distal (GLP-1) gut hormones on glucose and lipid metabolism in DIO rodents. Here we show that, (1) diet with high content of fat and sugar induces distinct and opposite effects in the growth and metabolism of the proximal versus distal gut, (2) morphologic and functional imbalance between

proximal and distal intestine is associated with a dysmetabolic phenotype, and (3) improved metabolic function after surgical and pharmacologic intervention is associated with restored balance between proximal and distal intestine. Our findings further support the role of the intestinal epithelium in the control of metabolism and suggest that interventions aimed at maintaining or restoring physiological balance between the proximal and the distal intestine may be effective ways to prevent and treat T2D and other metabolic diseases.

RESULTS

HFD Results in Opposite Effects on Intestinal Growth and Metabolism in the Proximal Versus Distal Gut

To determine the effect of HFD on the morphology and gene expression signatures of the gut, we fed mice HFD for up to 13 weeks and sampled segments of the small and large intestine. DIO mice had significantly higher body weight, fasting blood glucose (FBG), insulin, total cholesterol (TC) levels, and liver weight at 13 weeks compared with control mice ($p < 0.001$ for each; **Figure S1**).

Analysis of various segments of the gut via histologic imaging indicated that HFD causes hyperplasia of the mucosa of the proximal gut (the duodenum and the upper jejunum), while the distal gut (ileum) showed hypoplasia. Representative hematoxylin and eosin (H&E) stained sections illustrating changes in the dimension and morphology of the duodenum, jejunum, ileum, and colon are shown in **Figure 1A-E**. The mean (SE) duodenal weight was significantly increased in DIO mice compared with the control mice (172.2 [5.9] mg versus 151.9 [3.4] mg; $p < 0.001$). Similarly, the mean duodenum whole surface area (**Figure 1F**; $p < 0.001$) and volume (**Figure 1G**; $p < 0.05$) were significantly increased in DIO mice compared with control mice, indicative of a hyperplastic response to overnutrition. In contrast, the mean whole surface area of the distal small intestine (caudal jejunoileum [cJI]; p = not significant) and colon ($p < 0.001$), as well as the whole volume of the cJI ($p < 0.01$) and colon ($p < 0.001$) were lower (i.e., hypoplastic) in DIO mice compared with control mice. The increase in duodenal weight and volume was attributed to a significant increase in the duodenal mucosa (**Figure 1H**; $p < 0.05$), and not to an increase in the duodenal submucosa and muscularis (**Figure 1I**), while the

decrease in cJI and colon volume was attributed to a decrease of both the mucosa ($p < 0.01$) and submucosa and muscularis ($p < 0.001$).

In addition, the mean crypt density was significantly greater in the duodenum and jejunum of DIO mice compared with control mice ($p < 0.001$ for both segments; **Figure 1J**), suggesting an adaptive growth response by the stem cell compartment in response to nutrient overload, while no differences were noted in the ileum and colon. There was a significantly higher total number of GLP-1–positive enteroendocrine cells in the duodenum of DIO mice compared with chow-fed mice (**Figure 1K**; $p < 0.01$). As reported by others, however, the overall numbers of GLP-1–positive cells in the duodenum remained lower than those found in distal gut.(Hansen et al., 2013)

HFD also altered hormone expression across segments of the gut commensurate with the changes in mucosal thickness, with significantly higher mRNA levels of *Gip* ($p < 0.05$; **Figure 1L**) and cholecystokinin (*Cck*, $p < 0.05$; **Figure 1M**), both duodenum-specific hormones in the duodenum of DIO mice at 7 weeks compared with control mice. Pathway analyses on RNA-sequencing data from various segments of the small and large intestine suggested a robust impact of diet gut hormone production, as well as genes involved in cholesterol homeostasis, ketogenesis, glycolysis, fatty acid metabolism, oxidative phosphorylation, and immune response (including chemokine receptors) (**Figure 2**). Interestingly, the proximal gut (including the duodenum and jejunum) showed significant (adjusted false discovery rate [FDR; q value] < 0.25) changes in gene expression in response to DIO for many genes from these pathways; while, in general, their expression was not markedly impacted in distal segments of the intestine.

Nutrient Exposure Produces Differential Response in Duodenal Versus Ileal Organoids

Intestinal organoids are a three-dimensional, self-renewing, near physiological paradigm of the gut epithelium (Sato et al., 2009) that can be used to model the direct effects of a Westernized diet (i.e., excess saturated and trans fats and refined sugar) on gut mucosal growth and physiology. To model the impact of diet on the proximal versus distal gut, we derived mouse and human organoids from the duodenum and the terminal ileum of mice and human donors. We first assessed the impact of long-term lipid mixture (LM) exposure (4 weeks) on mouse duodenal and terminal ileal organoids. Notably, transcriptional responses diverged between mouse duodenal and ileal organoids in response to excess lipid. Stem cell marker *Lgr5* expression was numerically reduced in ileal but not duodenal organoids (**Figure S2A**). Expression of GIP and pre-proglucagon (*Gcg*; L-cell) genes, generally followed a similar pattern to that observed in DIO mice. *Gip* transcript increased in the duodenum in response to LM exposure but was significantly reduced in the ileum ($p < 0.05$) (**Figure S2B**), while pre-proglucagon RNA was significantly increased in the duodenum ($p < 0.0001$) and remained unchanged in the ileum (**Figure S2C**). EEC markers chromogranin A (*ChgA*) (**Figure S2D**) and cholecystokinin (*Cck*; **Figure S2E**) were numerically increased in the duodenum; however, *Cck* was numerically decreased in the ileum. Expression of secretin (*Sct*) (**Figure S2F**) and peptide YY (*Pyy*; **Figure S2G**) was unaltered in either gut segment.

In addition to proliferation, stem cell, and EEC changes, we noted differential impact of nutrients on other cell types in duodenal versus ileal organoids. The goblet cell marker, mucin 2 (*Muc2*) was significantly increased in duodenal ($p < 0.01$), but not ileal organoids (**Figure S2H**). Expression of enterocyte marker alkaline phosphatase (*Alpi*) (**Figure S2I**) was unchanged in duodenal organoids and significantly decreased in ileal organoids ($p < 0.01$). Paneth cell marker lysozyme (*Lyz1*) (**Figure S2J**) was unchanged in either gut segment.

We next turned to human duodenal and terminal ileal organoids to model the impact of either long-term lipid exposure or various concentrations of glucose on growth and stemness (self-renewal and differentiation) properties of each gut segment. While human intestinal organoids are relatively more stem-like in nature when compared with mouse small intestinal organoids, human intestinal organoids provide a biologically relevant platform to examine the effect of nutrients on stemness and mucosal growth.(Tsakmaki et al., 2017) Long-term exposure of organoids to LM significantly increased *LGR5* expression in the duodenal organoids ($p < 0.0001$) and, though to a lesser degree, in ileal organoids ($p < 0.01$) (**Figure 3A**), indicative of an increase in proliferating crypts. Similar to results in our *in vivo* study, the proliferation marker *Ki67* was significantly increased in duodenal organoids treated with LM compared with control ($p < 0.05$), while chronic exposure of ileal organoids to LM had no effect on *Ki67* (**Figure S3A**). Colony formation efficiency assays performed at weeks 2 and 4 of lipid exposure revealed significantly increased stemness in duodenal organoids in response to lipid (2 weeks, $p < 0.01$; 4 weeks, $p < 0.001$) (**Figure 3B**). Interestingly, this increased stemness was not observed in ileal organoids, indicative of a functionally different growth response profile of proximal versus distal intestine cell models to lipid. The expression of villin, an epithelial marker, mRNA was significantly reduced in duodenal and ileal organoids treated with LM compared with control ($p < 0.0001$ for both) (F**igure S3B**), whereas *LYZ1* expression, a marker of Paneth cells, was significantly reduced only in duodenal organoids ($p < 0.001$) (**Figure S3C**). *ALPI* expression, a marker of enterocytes, was significantly increased in ileal organoids ($p < 0.001$) treated with LM compared with control but was unchanged in duodenal organoids (**Figure S3D**).

Human organoids were next exposed to increasing concentrations of glucose across a physiological to pathophysiological range (5 mM [normoglycemia], 12 mM [prediabetes], and 25 mM [uncontrolled diabetes]). In duodenal organoids, high glucose concentrations significantly increased markers of proliferation, including *Ki67* (12 mM [$p < 0.0001$], 25 mM

[$p < 0.001$]) (**Figure 3C**) and proliferating cell nuclear antigen (*PCNA*; $p < 0.05$ for 12 mM and 25 mM) (**Figure 3D**). In addition, increasing concentrations of glucose increased the stem cell/early progenitor marker olfactomedin 4 (*OLFM4*) in duodenal organoids (12 mM [$p < 0.0001$], 25 mM [$p < 0.005$]) (**Figure 3E**), while *LGR5* appeared unchanged (**Figure 3F**). Glucose exposure also resulted in subtle but significant increases in villin mRNA expression in duodenal organoids (12 mM [$p < 0.01$], 25 mM [$p < 0.05$]) (**Figure 3G**), which suggests increases in growth due to glucose exposure. Long-term exposure to LM significantly increased peroxisome proliferator-activated receptor delta (*PPARD*) expression, important for uncoupling stem cells from their niche in high-fat feeding in duodenal ($p < 0.0001$), but not ileal organoids. **(Figure 3H)**.

In contrast, human ileal organoids responded to glucose in an opposite manner. High glucose concentrations reduced *Ki67* (25 mM [$p < 0.0001$]) (**Figure 3C**), *PCNA* (12 mM [$p < 0.001$], 25 mM [$p < 0.0001$]) (**Figure 3D**), *OLFM4* (25 mM [$p < 0.001$]) (**Figure 3E**), and *LGR5* expression ($p < 0.0001$ for 12 and 25 mM) (**Figure 3F**).

Altogether, the results from experiments using mouse and human organoid models provide evidence that the duodenal and ileal stem cell compartments differentially respond to excess lipid and glucose *in vitro*, supporting the observations of duodenal hyperplasia and ileal hypoplasia seen *in vivo*.

RYGB Surgery Elicits Morphologic and Hormonal Changes to Proximal Versus Distal Intestine that Oppose those Changes Seen in DIO Models

As exposure to a Westernized diet showed distinct responses in the proximal versus distal intestine both *in vitro* and *in vivo*, we next wanted to investigate the impact of excluding the

duodenum from nutrient passage on the morphology of and gene expression in the small intestines of DIO rodents. Therefore, we performed RYGB surgery to bypass the entire duodenum and proximal jejunum in rats that had been fed HFD for 20 weeks (DIO-RYGB). RYGB resulted in a rapid decrease in absolute (**Figure S4B**) and relative (**Figure 4A**) body weight in DIO rats starting on study day 2 ($p < 0.001$) compared with obese rats that underwent a sham procedure (DIO-Sham). As shown previously by others,(Lutz and Bueter, 2016) the reduction in body weight was sustained in DIO-RYGB rats, even in the presence of HFD, and was independent of food intake (DIO-RYGB versus DIO-Sham weight-matched [WM]) (**Figure S4C-E**).

Findings from stereology studies revealed that 3 weeks post-procedure, there was a significant increase in distal jejunum weight ($p < 0.001$) (**Figure 4B**) and proximal ($p < 0.01$) and distal ($p < 0.001$) jejunum volume (**Figure 4C**) in DIO-RYGB rats compared with DIO-Sham rats. In addition, results from immunohistochemistry analysis indicated that GIP cell density was reduced after RYGB in the alimentary (the branch of the "Y" through which food passes) and common (length of small intestine distal to site at which the two limbs join) limbs (**Figure 4D**). Consistent with reduced GIP cell density, the mean expression of other proximal intestinal gut hormones (including *Gip*, *Cck*, and ghrelin and obestatin prepropeptide [*Ghrl*]) were significantly downregulated following RYGB in the duodenum compared with a sham procedure ($p < 0.001$, $p < 0.05$, and $p < 0.01$, respectively) (**Figure 4E-G**), contrasting to the increase in GIP expression seen following administration of HFD in rats undergoing the sham procedure DIO-Sham.

To examine the differential effects of RYGB on proximal versus distal gut, we performed RNA sequencing on various segments of the small and large intestine and studied pathways significantly impacted by diet and RYGB (q value < 0.25). Similar to our DIO mouse gene

expression data, we noted a marked impact of HFD on the expression of genes responsible for gut hormone production, cholesterol homeostasis, glycolysis, and fatty acid and bile acid metabolism in the proximal gut, including the duodenum and jejunum (**Figure 5**). RYGB had a profound impact on expression of genes in these same pathways, with the proximal jejunum demonstrating the strongest effect post-RYGB, suggestive of the importance of local nutrient exposure on the molecular and cellular properties of each segment of the gut.(Ben-Zvi et al., 2018) Of note, RYGB often demonstrated opposite effects on gene expression when compared with DIO-sham. The increases in expression of gut hormones and genes involved in fatty acid and bile acid metabolism that were caused by HFD in the proximal gut were countered by large reductions in expression of these genes in the proximal gut after RYGB.

Taken together, these data show that RYGB led to opposing adaptive morphologic and gene expression changes in the proximal and distal gut that correlated with metabolic benefit compared with HFD on an anatomically intact bowel. Of note, gut hormones including the proximal gut hormone GIP and the distal gut hormone GLP-1 are differentially impacted because of the differential response of segments of the gut to HFD and/or RYGB.

GIP Receptor Antagonism Combined with GLP-1 Receptor Agonism Restores Metabolic Control in DIO mice

We next sought to alter the balance between proximal (GIP) and distal (GLP-1) gut hormones, using a pharmacological peptide-based approach, to investigate if these changes could counter the influence of HFD on the metabolic state.

We hypothesized that the differential changes in the proximal versus distal gut mucosa in response to HFD and/or RYGB may in part regulate overall metabolic homeostasis. Our data

along with data reported by others suggest that the GIP-to-GLP-1 activity ratio either increases in response to HFD or decreases due to RYGB. To revert the effects of HFD in DIO mice with a lower level of GIP signaling, as well as higher levels of GLP-1 (i.e., to pharmacologically mimic the effect of RYGB on these hormones), we investigated chronic pharmacologic antagonism of GIP with a prototypal GIP receptor (GIPR) antagonist GIP(3-30)NH2,(Sparre-Ulrich et al., 2017) in the absence and presence of pharmacologic GLP-1 receptor agonist liraglutide, on various measures of metabolism in DIO mice. Continuous subcutaneous infusion of GIPR antagonist alone or in combination with the GLP-1R agonist, given once daily, had no effect on absolute body weight (**Figure S5B**) or cumulative HFD intake (**Figure S5C**) compared with vehicle control. The GIPR antagonist alone worsened post-prandial glucose control as demonstrated by increased blood glucose levels after an oral glucose challenge (time 0), but it did not worsen the improved post-prandial control elicited by the GLP-1R agonist (**Figure 6A**). Mice treated with the GIPR antagonist in combination with the GLP-1R agonist had no difference in fasting glucose and numerically lower fasting insulin levels compared with mice treated with the GLP-1R agonist alone (**Figure 6B and C**). Homeostatic model assessment-insulin resistance (HOMA-IR) calculations obtained on study days 21 and 28 suggest that pharmacologic inhibition of the duodenal hormone GIP together with GLP-1R agonism reduces HFD-induced hyperinsulinemia and insulin resistance (**Figure 6D**).

In addition, a combination of the GIPR antagonist and the GLP-1R agonist resulted in significantly lower epididymal fat weight ($p < 0.05$) (**Figure 6E**) compared with the GLP-1R agonist administered alone. Plasma free fatty acids (**Figure 6F**), total cholesterol (TC) (**Figure 6G**), and plasma triglyceride (TG) (**Figure 6H**) levels were numerically lower in the combination group compared with the GLP-1R agonist administered alone.

Our data are further supported by others (Althage et al., 2008; Killion et al., 2018; Miyawaki et al., 2002) and show that differential perturbation of gut hormonal signals from the proximal and distal gut may have mutually reinforcing effects on metabolic homeostasis.

DISCUSSION

The Gut Plays a Critical Role in the Physiology and Pathophysiology of Endocrine and Metabolic Regulation

In this study, we investigated the effect of diet and intervention strategies on the proximal versus distal gut in rodent models as well as rodent and human organoids. Our data demonstrated that HFD results in different effects on cell growth, hormone expression, and metabolic signaling pathways in the proximal versus distal gut.

The adaptive response of the gut to nutrient availability is a well-known phenomenon. For example, total parenteral nutrition induces villus atrophy within days(Buchman et al., 1995), while surgical rearrangement of the gut causes hypertrophy in sections that, as a consequence of surgery, receive a greater nutrient load.(Dekaney et al., 2007; Feldman et al., 1976) Accordingly, jejunal villus height and crypt depth are increased in obesity (Mah et al., 2014) and are believed to be a consequence of the HFD uncoupling stem cells from their niche and thereby increasing stemness (Beyaz et al., 2016). Our work corroborates and extends this knowledge, demonstrating key differences in how the proximal versus distal gut respond to excess lipids or glucose.

We show that HFD induces adaptive responses in the duodenum, including mucosal hyperplasia and changes in the EEC population within the epithelium. HFD also profoundly impacts the intestinal transcriptome, with the expression of key genes. Notably, our data also show that duodenal hyperplasia in response to HFD is associated with hypoplasia and transcriptional adaptations of the distal small intestine (ileum) and colon.

Exposure of human organoids to excess lipids for 4-weeks augmented stemness accompanied with elevated *LGR5* expression in duodenal organoids when compared with ileal organoids. Hyperglycemic exposure (12 mM to 25 mM) increased expression of proliferation, stem cell and epithelial markers, and stemness in duodenal but not ileal organoids, suggesting the high lipid and glucose concentrations differentially influence duodenal versus ileal stem cells. We believe these results directly reflect *in vivo* observations of proximal gut overgrowth when rodents are exposed to a Western diet (excess trans-fat and refined sugar) and further validates the proximal hyperplasia versus distal hypoplasia findings. Our results suggest a possible link between the divergent effects of nutrients on epithelial growth, gut hormones and nutrient metabolism, and the dysmetabolic state. A key remaining question centers on why do proximal versus distal gut stem cells respond differently to nutrients? Is this a direct effect on the stem cell or via altered niche function? Further work is also needed to more directly establish the link between observed transcriptional changes and altered whole-body metabolism. The lack of fiber in the HFD relative to the fiber-rich control diet may also contribute to distal gut hypoplasia and transcriptional adaptations observed here; however, the effect of fiber was not directly investigated.

RYGB also has effects on local mucosal growth and hormone production in DIO rats, causing hyperplasia of the alimentary limb, stable weight loss, and metabolic benefit, despite continued exposure to HFD. The mucosal changes in RYGB are associated with decreased duodenal EEC hormonal signals as well as increases in key ileal EEC hormones (Sandoval, 2016). These effects are opposite those seen in our DIO mouse models and raised the critical question as to whether the balance between duodenal and ileal EEC hormonal changes are important in metabolic control.

GLP-1 receptor agonists are effective therapeutic agents to treat obesity and T2D, but they alone do not induce remission in diabetes, nor do they lead to the dramatic weight loss, seen from RYGB.(Amouyal and Andreelli, 2016) Our results suggest that peptide-based hormonal intervention with GIPR antagonists and GLP-1R agonists function together to improve the hyperinsulinemic and insulin-resistant state seen in DIO rat models. Of note, preclinical evidence reported by others suggests there is synergy between GIPR antagonism and GLP-1R agonism to improve insulin resistance and provide beneficial effects on lipid metabolism.(Killion et al., 2018)

Here, the GIPR antagonist administered alone does not affect body weight or dietary consumption. However, combination of GIPR antagonist with a GLP-1R agonist leads to improvements in metabolic parameters including reductions in fat mass, plasma FFA, and HOMA-IR, as well as trends in lowering total TG and TC levels, when compared with the GLP-1R agonist given alone. Of note, when administered alone, the GIPR antagonist worsens glucose control during a glucose challenge but had no effect when administered together with a GLP-1R agonist. Taken together, these data indicate that inhibition of GIPR in combination with GLP-1R agonism was associated with metabolic benefit in insulin levels and insulin resistance without compromising glucose control. Thus, GIPR inhibition provides a plausible explanation for weight-independent insulin sensitization seen after RYGB and other duodenal bypass interventions. Further, GIPR antagonism with GLP-1R agonism could work synergistically to improve the imbalance seen due to DIO, mimicking the improvements observed after RYGB.

Thus, methods which alter proximal versus distal gut biology, including RYGB and pharmacologic modulation of GIP and GLP-1 gut hormone signaling improved multiple metabolic parameters. Therefore, pathophysiological connection between the proximal and distal gut for the development of obesity, hyperinsulinemia, and systemic insulin resistance.

Additionally, these data may also offer a possible explanation for the apparent insulin-sensitizing effect observed with duodenal exclusion surgery and duodenal mucosal resurfacing interventions.

Balanced Equilibrium Model Describes the Role of Proximal Versus Distal Gut in Metabolic Homeostasis

In conjunction with the preclinical and clinical data already available in the literature, our data help establish the important, yet distinct roles of the proximal and distal small intestine in normal and pathophysiologic states. We postulate that duodenal hyperplasia in response to HFD, accompanied by ileal hypoplasia, results in a metabolic imbalance of proximal gut signals including enteroendocrine function versus distal gut signals that together contribute to the dysmetabolic state in obesity. With this framework, we believe gut hormones unique to each region play a prominent role, but other factors, such as lipid metabolism, neuronal signaling, microbiome effects, and bile acid signaling (Albaugh et al., 2019; Flynn et al., 2019; Wang et al., 2019), are also clearly important contributors and cannot be discounted. In addition, it has also been hypothesized that these effects may result from reducing putative “anti-incretin” signaling from the duodenum(Rubino et al., 2006; Rubino et al., 2004). Therefore, our model is important, but not comprehensive.

CONCLUSION

In summary, the intestine is topologically distinct longitudinally, highly adaptive to nutrient stimuli, and secretes diverse biologically active peptides and hormones that help regulate metabolism. Direct nutrient exposure induces differential changes in the proximal versus distal intestinal mucosa. Our results suggest Westernized high-calorie–dense diets induce organ-level changes of the intestinal epithelium (i.e., duodenal mucosal hyperplasia and ileal hypoplasia), which may be a causal mechanism driving insulin-resistant metabolic disease. Our balanced equilibrium model of metabolic homeostasis can therefore be applied to refine our understanding of metabolic disease pathogenesis and therapeutic development. Further understanding of the distinct properties of the proximal and distal segments of the small intestine will inform the design of procedures aimed at manipulating the physical maladaptation of intestinal segments or their corresponding hormones. Surgical, minimally invasive, or pharmacologic interventions that reverse the impact of duodenal hyperplasia and/or augment distal intestinal signaling may have significant benefit as rational therapeutic approaches in metabolic disease.

EXPERIMENTAL MODEL AND SUBJECT DETAILS

Animal Models and Maintenance

All animal experiments were performed according to Gubra's (Hørsholm, Denmark) bioethical guidelines, in compliance with internationally accepted laboratory animal care and use principles and monitored under personal licenses (2013-15-2934-00784 and 2015-15-0201-00518) issued by the Danish Animal Experimentation Council.

High-Fat, Diet-Induced Obese Mouse Model

C57Bl/6JRj mice (male, 6-weeks old; Janvier Labs, La Rochelle, France) were group housed under a 12:12 hour light-dark cycle and fed lean chow (Altromin #1324 [11% fat, 24% protein, 65% carbohydrate], Brogaarden, Denmark) or HFD (SSNIFF® diet #12492 [60% fat, 20% protein, 20% carbohydrate], Soest, Germany) for 7 or 13 weeks. Body weight was measured and recorded at baseline (week 0), week 7, and week 13. Mice were sacrificed per protocol by an overdose of isoflurane followed by heart bleeding.

High-Fat, Diet-Induced Obese Rat Model

Sprague Dawley rats (male, 27-weeks old; Taconic Biosciences, Ejby, Denmark) were group housed under a 12:12 hour light-dark cycle and fed a two-choice diet of HFD (Gubra diet made from equal amounts of chocolate spread [Nutella, Ferrero, Pino Torinese, Italy], peanut butter [Swartberg, PCD, AJ Rotterdam, Nederland], and powdered rodent chow [#1320, Altromin, Lage, Germany]; 29.3% fat, 33.2% carbohydrate, and 18% protein) and pelleted chow (#1324, Altromin, Lage, Germany) ad libitum for 20 weeks before being randomized 1:3 to receive either RYGB or sham procedure (described below) at baseline (day 0) (**Figure S3A**). Post-procedure, rats were individually housed to monitor food intake. Rats were fed a liquid diet (Fresubin

Original, Fresenius Kabi, Bad Homburg, Germany [4.2 kJ/mL, fat 3.4%, carbohydrate 13.8%, and protein 3.8%]) from day –3 to day 11, and were again offered HFD and chow from days 11 to 21 (study termination). Body weight (from day 0 to 21), food intake (from day –2 to 21), results of gut histology and stereology, and global gene expression were analyzed in the following four groups: (1) Rats undergoing sham procedure were fed HFD and chow from days 11 to 21 (Sham/DIO group); (2) rats undergoing RYGB were fed HFD and chow from days 11 to 21 (RYGB/DIO group); (3) rats undergoing sham procedure were fed HFD and chow from days 11 to 21, weight-matched with RYGB/DIO (Sham/DIO/WM group); and (4) lean rats undergoing sham procedure were fed chow from days 11 to 21 (Sham/Lean group). On day 21, all animals were sacrificed by cardiac bleeding under isoflurane anesthesia.

Blood Pharmacology

Cardiac blood was sampled using a needle and vacuette (9 mL 23 G syringe [rats], 1 mL 25G needle [mice]) directly from the left ventricle. Tail and tongue blood samples were collected in 10 µL heparinized glass capillary tubes, and directly transferred into an Eppendorf tube with a buffer and shaken before blood glucose (BG) measurement. Fasting blood glucose (FBG) was measured using a BIOSEN c-Line glucose meter (EKF-Diagnostics, Barleben, Germany), insulin was measured using the Meso Scale Diagnostics platform, TG and TC were measured using commercial kits (Roche Diagnostics, Mannheim, Germany) on the Cobas C-501 autoanalyzer (Roche, Switzerland), and free fatty acid (FFA) levels were measured using a Wako Chemicals kit (Richmond, VA) on the Cobas C-501 autoanalyzer, all according to the

manufacturers' instructions. Homeostatic model assessment-insulin resistance (HOMA-IR) was calculated using the following equation:

$$(\text{fasting insulin concentration [pmol/L]}) \times (\text{fasting glucose concentration [mmol/L]})/22.5.$$

Oral Glucose Tolerance Test

Animals were fasted 4 hours before oral glucose administration (2 g/kg). Blood glucose was measured at –30, 0, 15, 30, 60, 120, and 180 minutes after glucose administration, and insulin was measured at 0 and 30 minutes after glucose administration. Blood samples were collected in 10 µL heparinized glass capillary tubes and blood glucose was measured as described above.

Stereology and Histology

Detailed stereological analysis was conducted along the length of the gastrointestinal tract with mucosal surface staining using standard procedures. Briefly, formalin-fixed small intestine, anatomically divided into the duodenum (pyloric sphincter to duodenojejunal bend), and jejunoileum (duodenojejunal bend to caecum) and large intestine were sampled using the systematic random uniform sampling principle, then embedded in paraffin. Paraffin-embedded gut tissue was sectioned (5 µm), mounted on Superfrost+ glass slides, de-paraffinized in xylene, and rehydrated in graded ethanol. For hematoxylin and eosin staining, slides were incubated in hematoxylin (Dako, Agilent), washed in tap water, stained with eosin Y (Sigma-Aldrich St. Louis, MO, USA), hydrated, mounted with Pertex mounting medium (International Medical Products, Belgium), and then allowed to dry. Immunohistochemistry was performed using standard procedures. Briefly, after antigen retrieval and endogenous peroxidase activity blocking, tissue sections were incubated in primary antibody. Primary antibodies were detected and amplified

using a horseradish peroxidase polymer system and visualized with 3,3'-diaminobenzidine as chromogen, using hematoxylin as a counterstain.

Stereological volume and cell number were estimated using the newCAST system (Visiopharm, Denmark). Total gut volume and mucosa and submucosa plus muscularis volume were estimated by point counting using a grid system, where points hitting the structure of interest were counted and converted into volume using the following equation:

$$vol_{ref} = \sum p \times A(p) \times t,$$

where A(p) indicates area per point; p, total number of points hitting the structure of interest; and t, the distance between sections. The physical dissector principle was used to perform cell number estimates. Briefly, for each section, region of interest (ROI) was defined using ROI delineation. The disector counting frame and sampling frequency were adjusted to allow for an average of 150 cells to be identified in ~100 disectors/animal/ROI. Total number of cells were counted, and particle density N_v was calculated using the following equation:

$$N_v = (1/(A(_{frame}) \times h)) \times ((\sum Q^-)/(\sum P)),$$

where $A(_{frame})$ indicates area of the disector counting frame; h, disector height; $\sum P$, total number of points hitting the reference volume; and $\sum Q$, total number of positive cells counted. The total number of positive cells equal $N_v \times V_{reference}$. Crypt density was manually counted by an investigator blinded to the intervention and calculated by dividing the number of well-orientated

crypts per millimeter of submucosal circumference. Six matched sections covering on average 15 mm of mucosa were analyzed per segment per animal.

RNA Sequencing

Transcriptomic analyses of both the gut and liver were performed. Tissue samples were lysed using the MP FastPrep system (MP Biomedicals, Solon, OH, USA). RNA extraction was performed using NucleoSpin Plus RNA columns (Macherey-Nagel, Düren, Germany), RNA was quantified using a NanoDrop 2000 spectrophotometer (Thermo Fisher Scientific, Waltham, MA, USA), and purified RNA was stored at –80ºC. Up to 1 µg of purified RNA from each sample was used to create a cDNA library with the NEBNext Ultra II Directional RNA Library Prep Kit or NextSeq 500/550 High Output Kit v2 for sequencing on a NextSeq 500 (Illumina, San Diego, CA, USA). The Spliced Transcripts Alignment to a Reference (STAR) software (Dobin et al., 2013) (Illumina; San Diego, CA, USA) was used to align sequencing data to the mouse or rat genome from the Ensembl 89 genome browser database. Data quality was evaluated using standard quality control parameters. Inter- and intra-group variability were assessed via principal component analysis and hierarchical clustering. Differentially expressed genes were identified with R-package DESeq2 (Bioconductor).

Intestinal Organoids

Mouse and Human Intestinal Crypt Isolation and Culturing

Mouse duodenal and terminal ileum crypts were isolated and grown into organoids as described by Sato et al, 2009.(Sato et al., 2009) Human duodenal and terminal ileum crypts were isolated from biopsies from two different patients undergoing endoscopy at Guy’s and St Thomas’ NHS Foundation Trust, after giving written, informed consent (National Research Service ID 190309).

Crypts from those biopsies were isolated and grown into organoids as described by Fujii et al.(Fujii et al., 2015)

Mouse crypts were cultured in growth culture medium containing advanced DMEM/F12, penicillin/streptomycin (100 units/mL), 10 mM HEPES, 2 mM Glutamax, supplements N2 (1×) and B27 (1×), 50 ng/mL mouse epidermal growth factor (all Gibco, Thermo Fisher Scientific), 1 mM N-acetylcysteine (Sigma-Aldrich; St. Louis, MO, USA), 100 ng/mL Noggin (Peprotech, Rocky Hill, NJ, USA), and 10% volume/volume R-spondin-1–conditioned medium. R-spond-1-producing cell line was a kind gift from Dr. Calvin Kuo.

Human growth medium additionally contained 50% Wnt3A-conditioned medium, 10 nM gastrin (Sigma-Aldrich), 500 nM A83-01 (Bio-Techne, Minneapolis, MN, USA), 10 µM SB202190 (Sigma-Aldrich), and 10 mM nicotinamide (Sigma-Aldrich). Differentiation of human organoids toward a mature epithelium was achieved with reduction of Wnt3a-conditioned medium to 15% and withdrawal of SB202190 and nicotinamide from the culture medium. L-Wnt3A cells for production of Wnt3A-conditioned medium were a kind gift from Dr. Hans Clever.

A long-term lipid mixture (LM) was added to the growth medium of mouse and human organoids in a final concentration of 2% (Sigma-Aldrich, L0288) for 4 weeks.

To expose human organoids to different levels of glucose, the Advanced DMEM/F12 medium/F12 was replaced with glucose-free SILAC Advanced DMEM/F-12 Flex Medium supplemented with 147.5 mg/L L-arginine and 91.25 mg/L L-Lysine (Sigma-Aldrich). Human organoids were split and kept in growth medium with 5 µM Chiron and 10 µM Y-27632 dihydrochloride monohydrate (both from Sigma-Aldrich) for 3 days before being transferred into differentiation medium with increased amounts of glucose (5.5, 12, and 25 mM) for 4 to 7 days.

Colony-Forming Efficiency

Human organoids were cultured for 2 or 4 weeks in the presence or absence of 2% LM, then dissociated with TrypLE Express (Gibco Laboratories, Gaithersburg, MD, USA), and 1000 single cells embedded in Matrigel were plated in each well. Single cells were cultured in normal growth medium without LM, and the number of organoids in each well was measured on day 10.

Quantitative Real-Time Polymerase Chain Reaction

Total RNA was extracted from mouse and human organoids using RNeasy mini kit (Qiagen, Hilden, Germany). RNA was converted to cDNA using a high-capacity cDNA reverse transcription kit (Life Technologies, Carlsbad, CA, USA). Gene expression levels were quantified using QuantiTect primers and Quantitect SybrGreen MasterMix (both from Qiagen) on a LightCycler 480 (Roche, Basel, Switzerland). Samples were analyzed in duplicates and relative expression of mRNAs were determined after normalization against Beta-2-Microglobulin. Statistical significance was evaluated using one-way analysis of variance with multiple comparisons.

Rodent Surgical Procedures

Pharmacological Studies of GIPR Antagonism and GLP-1 Agonism in DIO Mice

C57BL/6JRj mice (23-week-old males, Janvier Labs, La Rochelle, France) were individually housed under 12:12 hour light-dark cycle (lights off at 3:00 pm) and fed HFD (SSNIFF® diet #12492) for 18 weeks before and during the study (**Figure S3A**).

Alzet 100 µL minipumps (Alzet, Cupertino, CA, USA) were filled with GIP(3-30)NH2 (30 mg/mL) or vehicle 2 (DMSO/propylene glycol [50/50 volume per volume]) and kept in 0.9% saline at

37°C overnight. The minipump was placed subcutaneously (SC) through a 1-cm long incision in the neck with the animal under isoflurane anesthesia, and the incision was closed using a 6-0 Ethicon II (Ethicon, Somerville, New Jersey, USA) suture, as previously described.(Lu et al., 2015) From day 0 (first dose) through day 28, mice received one of the following four treatments: (1) vehicle 1 (phosphate-buffered saline [PBS] plus 0.1% bovine serum albumin [BSA], SC, once daily [QD]) and continuous infusion of vehicle 2 via osmotic minipump; (2) glucagon-like peptide-1 receptor (GLP-1R) agonist (0.2 mg/kg liraglutide, SC, QD, Victoza (Novo Nordisk, Bagsværd, Denmark) and continuous infusion of vehicle 2 via osmotic minipump; (3) vehicle 1 (SC, QD) and continuous infusion of a glucose-dependent insulinotropic polypeptide receptor (GIPR) antagonist (~4.5 mg/kg/day / 56.8 nmol/kg/h GIP[3-30]NH2, CPC Scientific Inc, Sunnyvale, CA, USA) via osmotic minipump; and (4) GLP-1R agonist (0.2 mg/kg liraglutide, SC, QD) and continuous infusion of GIPR antagonist (~4.5 mg/kg/day GIP[3-30]NH2) via osmotic minipump.

Roux-en-Y Gastric Bypass

RYGB or sham procedures were performed after an overnight fast with animals under isoflurane anesthesia, as previously described,(Chambers et al., 2011) with the only modification being that the length of the alimentary limb was 30 cm and the biliopancreatic limb was 15 cm. Sham surgeries were created by removing the gut and stomach from the abdominal cavity, as done in the RYGB surgery, and placing it back without making any incisions.

Statistical Analysis for Animal Models

High-Fat, Diet-Induced Obese Mouse

Statistical significance was evaluated using one-way (FBG, insulin, TC, and liver weight) or two-way (body weight) analysis of variance, or unpaired *t* test (volume measurements by gut region and surface area, GLP-1 cell number and density). *Post hoc t* tests were performed with correction for multiple comparisons using the Bonferroni method. A cutoff of $p < .05$ was used as a threshold for statistical significance. For continuous data from minipump experiments with a single time point or repeated measures, a one-factor linear model was used to compare difference in plasma insulin, TG, TC, FFA, and epididymal fat weight between treatments and control using Dunnett's test. A 2×2 contingency table consisting of responders and non-responders in control and treatment groups was used to analyze categorical data, and a Fisher's exact test was used for all pairwise comparisons with *p* values adjusted using the Bonferroni correction.

High-Fat, Diet-Induced Obese Rat

Significant differences between treatment groups was determined using Dunnett's test one-factor (total body weight, total gut weight and volume, mucosal weight) linear model of last study day data or two-factor (intestinal weight and volume in different intestinal regions) linear model with interaction.

Pathway Analysis

Pathway analyses were performed using Gene Set Enrichment Analysis (GSEA) to determine if members of a gene set defined *a priori* were perturbed among the differentially expressed genes, as previously described.(Mootha et al., 2003) This method leverages gene sets categorized by biological pathways to improve statistical power and increase signal relative to noise. A simplified schematic overview of the GSEA first describes the ordering of collected RNA-Seq data into a ranked ordered pathway gene set *S*, by expression difference between

two physiological states using signal to noise as the appropriate distance metric and relationship to a pathway. A Kolmogrov-Smirnov running sum statistic, termed the enrichment score, was computed to identify whether top-ranked genes are enriched in the pathway gene set *S*. KEGG and Hallmark pathway gene sets were used for gene expression profiling between two biological states along various intestine regions in the mouse and rat studies. Using actual data, the enrichment score was computed for every pathway gene set and a maximum enrichment score (MES) was recorded. The steps were repeated 1000 times, which involved randomization of the diagnostic/class labels, to determine whether one or more pathways are perturbed in one class and used to build a histogram of permuted MES. The significance of the permuted MES was evaluated against the actual MES, providing a global *p* value for whether any gene set is perturbed within a class. A gene set with nominal p value $< .05$ and false discovery rate < 0.25 was considered significant.(Glickman et al., 2014) The sample size for each experiment and information about the statistical tests that were used are reported in each figure legend.

FIGURE LEGENDS

Figure 1. HFD-Induced Adaptive Responses in Mouse Intestinal Mucosa, Enteroendocrine Cell Numbers, and Transcriptional Changes in Gut Hormones

Representative hematoxylin and eosin–stained cross-sections of duodenum, jejunum, ileum, and colon from mice fed lean chow (CTRL) (A – E) or HFD (A' – E'). Scale bar = 1000 µm, unless otherwise noted. The mucosal layer is bracketed in panels A and A'. Whole intestine surface area in cm^2 (F), whole intestine volume in mm^3 (G), mucosa volume in mm^3 (H), and submucosa and muscularis volume in mm^3 (I) estimated by stereology in mice following consumption of CTRL chow or HFD (DIO) for 13 weeks by intestinal region. (J) Histologic quantification of crypt density (number/mm) in DIO and CTRL groups at 13 weeks. Whole intestine GLP-1–positive cell number (K) by intestinal region in CTRL or DIO mice at 13 weeks. mRNA expression levels of *GIP* (L) and *CCK* (M) by intestinal region (13-week data presented for rJI, cJI, and colon regions). Data are presented as mean ± standard error of the mean. Statistical significance was evaluated using unpaired *t* test with ***$p < 0.001$, **$p < 0.01$, and *$p < 0.05$. cJI, caudal jejunoileum; CCK, cholecystokinin; CTRL, control; DIO, diet-induced obesity; GIP, glucose-dependent insulinotropic polypeptide; GLP-1, glucagon-like peptide-1; HFD, high-fat diet; rJI, rostral jejunoileum; RPKM, reads per kilobase per million sequence reads.

Figure 2. HFD-Induced Expression Changes in Metabolic and Immune Response Pathways

Heat map of mean log2-fold change in expression levels of genes linked to pathways perturbed by an HFD versus lean chow (control) in samples from duodenum at 7 weeks and from duodenum, jejunum, ileum, colon, and liver at 13 weeks post-initiation of dietary intervention. Pathway (gene sets of Hallmarks/KEGG pathways) expression in the duodenum at 7 weeks (n = 10), and duodenum (n = 10), jejunum/rJI (n = 8), ileum/cJI (n = 6), colon (n = 8), and liver (n = 8) at 13 weeks was compared between mice fed with HFD or control with an adjusted FDR *p* value (q value) < 0.25 considered significant. A significant impact of diet was found in the rJI for gene pathways related to fatty acid metabolism, oxidative phosphorylation, glycolysis/gluconeogenesis, and bile acid metabolism. cJL, caudal jejunoileum; HFD, high-fat diet; FDR, false discovery rate; KEGG, Kyoto encyclopedia of genes and genomes; rJI, rostral jejunoileum.

Figure 3. Divergent Growth and Transcriptional Responses of Human Duodenal and Ileal Organoids to Lipid and Glucose Treatment

(A) *LGR5* expression in human duodenal and ileal organoids after 4 weeks of 2% lipid exposure. (B) Organoid colony formation efficiency assays performed at weeks 2 and 4 of 2% lipid exposure, revealing significantly increased stemness in duodenal but not in ileal organoids. Impact of exposure of human duodenal and ileal organoids to increased concentrations of glucose (5.5 mM, 12 mM, and 25 mM) on mRNA expression levels of *Ki67* (C); *PCNA* (D); *OLFM4* (E); *LGR5* (F), and Villin (G). *PPAR-d* expression in human duodenal and ileal organoids after 4 weeks of 2% lipid exposure. All gene expression values are presented relative to B2M gene transcript (H). Data are presented as mean ± SEM. Statistical significance in lipid mixture experiments was evaluated using unpaired *t* test and in glucose experiments using one-way ANOVA with *$p < 0.05$; **$p < 0.01$; ***$p < 0.001$; ****$p < 0.0001$. ANOVA, analysis of variance; B2M, beta-2-microglobulin; CTRL, control; *LGR5*, leucine-rich repeat-containing G-protein-coupled receptor 5; LM, lipid mixture; *OLFM4*, olfactomedin 4; *PPAR-d*, peroxisome proliferator–activated receptor delta; *PCNA*, proliferating cell nuclear antigen; SEM, standard error of the mean; wks; weeks.

Figure 4. Roux-en-Y Gastric Bypass Surgery in Diet-Induced Obesity Rat Model Establishes the Importance of the Proximal and Distal Gut Morphology and Gene Expression

(A) Relative body weight from day 0 to 21. (B) Gut weight (milligrams) by region. (C) Gut volume (millimeter^3) by region. (D) Representative images of GIP immunohistochemistry staining (Magnification = 10x). *Gip* (D), *Cck* (E), and *Ghrl* (F) mRNA expression levels by gut region. Data are presented as mean (standard error of the mean [SEM]), unless otherwise noted. *Cck,* cholecystokinin; DIO, diet-induced obesity; *Ghrl*, ghrelin and obestatin prepropeptide; *Gip*, glucose-dependent insulinotropic polypeptide; RYGB, Roux-en-Y gastric bypass. *$p < 0.05$; **$p < 0.01$; ***$p < 0.001$ after correction for gene-wise multiple testing. N = 10 for each group.

Figure 5. Roux-en-Y Gastric Bypass Affects the Gene Expression in Metabolic Regulation Pathways Distinctly in Proximal Versus Distal Segments of the Intestine

Heat map of mean log2-fold change expression levels of genes linked to pathways found to be perturbed by either DIO-sham or DIO-RYGB versus lean-sham controls (adjusted FDR *p* value < 0.25 considered significant). A significant impact of RYGB was found in the proximal jejunum for gene pathways related cholesterol homeostasis. Labeling was simplified based on the following: Duodenum for both duodenum in sham control animals or biliopancreatic limb after RYGB, proximal jejunum for both proximal jejunum in sham-controlled animals, and alimentary limb after RYGB, proximal jejunum for both proximal jejunum in sham animals, and common channel after RYGB. DIO, diet-induced obesity; FDR, false discovery rate; RYGB, Roux-en-Y gastric bypass. N = 10 for each group.

Figure 6. The Effect of GIPR Antagonism via GIP(3-30)NH2 in Combination with Liraglutide on Glucose and Lipid Homeostasis in DIO Mice

(A) Blood glucose (millimoles/liter) during the OGTT on day 21 measured at –30, 0, 15, 30, 60, 120, and 180 minutes relative to oral glucose load (time 0). Animals were dosed at –30 minutes. (B) Percent change in blood glucose (millimoles/liter) from day –3 to day 28. (C) Mean (SE) percent change in fasting insulin from day –3 to day 28. (D) Percent change in HOMA-IR from day –3 to day 21 and from day –3 to day 28. (E) Mean (interquartile range) terminal epididymal fat weight relative to body weight. (F) Mean (interquartile range) plasma free fatty acids (micromoles/liter) at termination. (G) Median (interquartile range) of plasma TC (millimoles/liter) at termination. (H) Median (interquartile range) of plasma TG (millimoles/liter) at termination. Data are presented as mean ± SEM, unless otherwise noted. For continuous data from minipump experiments with a single time point or repeated measures, a one-factor linear model was used to compare difference in plasma insulin, TG, TC, FFA, and epididymal fat weight between treatments and control using Dunnett's test. A 2 x 2 contingency table consisting of responders and non-responders in control and treatment groups was used to analyze categorical data, and a Fisher's exact test was used for all pairwise comparisons with p values adjusted using the Bonferroni correction. *$p < 0.05$; **$p < 0.01$; ***$p < 0.001$ compared with vehicle. GIP, glucose-dependent insulinotropic polypeptide; GLP-1, glucagon-like peptide-1; HOMA-IR, homeostatic model assessment-insulin resistance; OGTT, oral glucose tolerance test; TC, total cholesterol; TG, triglycerides. N = 10 for each group.

ACKNOWLEDGMENTS

This study was supported by Fractyl Laboratories Inc Lexington, MA. The authors would like to thank Jay Caplan, Alice P Liou, and Vijeta Bhambhani for critical review of this manuscript. Medical writing support, funded by Fractyl Laboratories Inc, was provided by Caroline W Cazares, PhD, of JB Ashtin, who developed the first draft based on an author-approved outline and assisted in implementing author revisions.

AUTHOR CONTRIBUTIONS

Conceptualization and methodology, J.A.W., S.S.G., D.G.P., D.M., G.A.B., and H.R.; Investigation, A.T., P.W., K.T.G.R., P.J.P., D.M. G.A.B., H.R., and P.P.; Formal analysis and writing, review, and editing, J.A.W., S.S.G., D.G.P., A.T., P.W., K.T.G.R., P.J.P., D.M., G.A.B., H.R., and J.C.L.T. All authors reviewed and critiqued the manuscript throughout the editorial process, approved the final manuscript draft submitted for publication, and agreed to be accountable for all aspects of the work, ensuring the accuracy and integrity of the publication.

DECLARATION OF INTERESTS

SSG has received honorarium for consultancy from Fractyl Laboratories Inc.

AT has received funding/grant support from JDRF.

PW, **KTGR**, and **PJP** are employees of Gubra ApS.

DGP has received honorarium for consultancy from Fractyl Laboratories Inc.

PP has received funding/grant support from CCUK, GutsUK, King's Health Partners and the Rosetrees Trust.

DM is an ex-employee of Fractyl Laboratories Inc., is a current shareholder, and has received honorarium for consultancy from Fractyl Laboratories Inc.

HR, **JAW**, **JCLT** and **JHSH** are employees and shareholders of Fractyl Laboratories Inc.

GAB has received funding/grant support from EFSD and JDRF and honorarium for consultancy from Fractyl Laboratories Inc.

Data Sharing Statement

The datasets generated during and/or analyzed during the current study are available from the corresponding author on reasonable request.

REFERENCES

Adachi, T., Mori, C., Sakurai, K., Shihara, N., Tsuda, K., and Yasuda, K. (2003). Morphological changes and increased sucrase and isomaltase activity in small intestines of insulin-deficient and type 2 diabetic rats. Endocrine journal *50*, 271-279.

Albaugh, V.L., Banan, B., Antoun, J., Xiong, Y., Guo, Y., Ping, J., Alikhan, M., Clements, B.A., Abumrad, N.N., and Flynn, C.R. (2019). Role of Bile Acids and GLP-1 in Mediating the Metabolic Improvements of Bariatric Surgery. Gastroenterology *156*, 1041-1051 e1044.

Althage, M.C., Ford, E.L., Wang, S., Tso, P., Polonsky, K.S., and Wice, B.M. (2008). Targeted ablation of glucose-dependent insulinotropic polypeptide-producing cells in transgenic mice reduces obesity and insulin resistance induced by a high fat diet. The Journal of biological chemistry *283*, 18365-18376.

Amouyal, C., and Andreelli, F. (2016). Increasing GLP-1 Circulating Levels by Bariatric Surgery or by GLP-1 Receptor Agonists Therapy: Why Are the Clinical Consequences so Different? J Diabetes Res *2016*, 5908656.

Bailey, C.J., Flatt, P.R., Kwasowski, P., Powell, C.J., and Marks, V. (1986). Immunoreactive gastric inhibitory polypeptide and K cell hyperplasia in obese hyperglycaemic (ob/ob) mice fed high fat and high carbohydrate cafeteria diets. Acta endocrinologica *112*, 224-229.

Barker, N., van Es, J.H., Kuipers, J., Kujala, P., van den Born, M., Cozijnsen, M., Haegebarth, A., Korving, J., Begthel, H., Peters, P.J., et al. (2007). Identification of stem cells in small intestine and colon by marker gene Lgr5. Nature *449*, 1003-1007.

Ben-Zvi, D., Meoli, L., Abidi, W.M., Nestoridi, E., Panciotti, C., Castillo, E., Pizarro, P., Shirley, E., Gourash, W.F., Thompson, C.C., et al. (2018). Time-dependent molecular responses differ between gastric bypass and dieting but are conserved across species. Cell metabolism *28*, 310-323 e316.

Beyaz, S., Mana, M.D., Roper, J., Kedrin, D., Saadatpour, A., Hong, S.J., Bauer-Rowe, K.E., Xifaras, M.E., Akkad, A., Arias, E., et al. (2016). High-fat diet enhances stemness and tumorigenicity of intestinal progenitors. Nature *531*, 53-58.

Buchman, A.L., Moukarzel, A.A., Bhuta, S., Belle, M., Ament, M.E., Eckhert, C.D., Hollander, D., Gornbein, J., Kopple, J.D., and Vijayaroghavan, S.R. (1995). Parenteral nutrition is associated with intestinal morphologic and functional changes in humans. JPEN J Parenter Enteral Nutr *19*, 453-460.

Chambers, A.P., Jessen, L., Ryan, K.K., Sisley, S., Wilson-Perez, H.E., Stefater, M.A., Gaitonde, S.G., Sorrell, J.E., Toure, M., Berger, J., et al. (2011). Weight-independent changes in blood glucose homeostasis after gastric bypass or vertical sleeve gastrectomy in rats. Gastroenterology *141*, 950-958.

Cordain, L., Eaton, S.B., Sebastian, A., Mann, N., Lindeberg, S., Watkins, B.A., O'Keefe, J.H., and Brand-Miller, J. (2005). Origins and evolution of the Western diet: health implications for the 21st century. The American journal of clinical nutrition *81*, 341-354.

Cummings, D.E., and Overduin, J. (2007). Gastrointestinal regulation of food intake. J Clin Invest *117*, 13-23.

Cummings, D.E., Overduin, J., Foster-Schubert, K.E., and Carlson, M.J. (2007). Role of the bypassed proximal intestine in the anti-diabetic effects of bariatric surgery. Surgery for obesity and related diseases : official journal of the American Society for Bariatric Surgery *3*, 109-115.

Danaei, G., Singh, G.M., Paciorek, C.J., Lin, J.K., Cowan, M.J., Finucane, M.M., Farzadfar, F., Stevens, G.A., Riley, L.M., Lu, Y., et al. (2013). The global cardiovascular risk transition: associations of four metabolic risk factors with national income, urbanization, and Western diet in 1980 and 2008. Circulation *127*, 1493-1502, 1502e1491-1498.

de Jonge, C., Rensen, S.S., Verdam, F.J., Vincent, R.P., Bloom, S.R., Buurman, W.A., le Roux, C.W., Schaper, N.C., Bouvy, N.D., and Greve, J.W. (2013). Endoscopic duodenal-jejunal bypass liner rapidly improves type 2 diabetes. Obesity surgery *23*, 1354-1360.

de Wit, N.J., Bosch-Vermeulen, H., de Groot, P.J., Hooiveld, G.J., Bromhaar, M.M., Jansen, J., Muller, M., and van der Meer, R. (2008). The role of the small intestine in the development of dietary fat-induced obesity and insulin resistance in C57BL/6J mice. BMC medical genomics *1*, 14.

Dekaney, C.M., Fong, J.J., Rigby, R.J., Lund, P.K., Henning, S.J., and Helmrath, M.A. (2007). Expansion of intestinal stem cells associated with long-term adaptation following ileocecal resection in mice. Am J Physiol Gastrointest Liver Physiol *293*, G1013-1022.

Dobin, A., Davis, C.A., Schlesinger, F., Drenkow, J., Zaleski, C., Jha, S., Batut, P., Chaisson, M., and Gingeras, T.R. (2013). STAR: ultrafast universal RNA-seq aligner. Bioinformatics *29*, 15-21.

Feldman, E.J., Dowling, R.H., McNaughton, J., and Peters, T.J. (1976). Effects of oral versus intravenous nutrition on intestinal adaptation after small bowel resection in the dog. Gastroenterology *70*, 712-719.

Ferrannini, E., and Mingrone, G. (2009). Impact of different bariatric surgical procedures on insulin action and beta-cell function in type 2 diabetes. Diabetes care *32*, 514-520.

Flynn, C.R., Albaugh, V.L., and Abumrad, N.N. (2019). Metabolic Effects of Bile Acids: Potential Role in Bariatric Surgery. Cell Mol Gastroenterol Hepatol *8*, 235-246.

Fujii, M., Matano, M., Nanki, K., and Sato, T. (2015). Efficient genetic engineering of human intestinal organoids using electroporation. Nature protocols *10*, 1474-1485.

Gehart, H., van Es, J.H., Hamer, K., Beumer, J., Kretzschmar, K., Dekkers, J.F., Rios, A., and Clevers, H. (2019). Identification of enteroendocrine regulators by real-time single-cell differentiation mapping. Cell *176*, 1158-1173 e1116.

Glickman, M.E., Rao, S.R., and Schultz, M.R. (2014). False discovery rate control is a recommended alternative to Bonferroni-type adjustments in health studies. Journal of clinical epidemiology *67*, 850-857.

Gniuli, D., Calcagno, A., Dalla Libera, L., Calvani, R., Leccesi, L., Caristo, M.E., Vettor, R., Castagneto, M., Ghirlanda, G., and Mingrone, G. (2010). High-fat feeding stimulates endocrine, glucose-dependent insulinotropic polypeptide (GIP)-expressing cell hyperplasia in the duodenum of Wistar rats. Diabetologia *53*, 2233-2240.

Gribble, F.M., and Reimann, F. (2019). Function and mechanisms of enteroendocrine cells and gut hormones in metabolism. Nature reviews. Endocrinology *15*, 226-237.

Haber, A.L., Biton, M., Rogel, N., Herbst, R.H., Shekhar, K., Smillie, C., Burgin, G., Delorey, T.M., Howitt, M.R., Katz, Y., et al. (2017). A single-cell survey of the small intestinal epithelium. Nature *551*, 333-339.

Hansen, C.F., Vrang, N., Sangild, P.T., and Jelsing, J. (2013). Novel insight into the distribution of L-cells in the rat intestinal tract. American journal of translational research *5*, 347-358.

Jacobsen, S.H., Olesen, S.C., Dirksen, C., Jorgensen, N.B., Bojsen-Moller, K.N., Kielgast, U., Worm, D., Almdal, T., Naver, L.S., Hvolris, L.E., et al. (2012). Changes in gastrointestinal hormone responses, insulin sensitivity, and beta-cell function within 2 weeks after gastric bypass in non-diabetic subjects. Obesity surgery *22*, 1084-1096.

Jirapinyo, P., Haas, A.V., and Thompson, C.C. (2018). Effect of the duodenal-jejunal bypass liner on glycemic control in patients with type 2 diabetes with obesity: a meta-analysis with secondary analysis on weight loss and hormonal changes. Diabetes care *41*, 1106-1115.

Killion, E.A., Wang, J., Yie, J., Shi, S.D., Bates, D., Min, X., Komorowski, R., Hager, T., Deng, L., Atangan, L., et al. (2018). Anti-obesity effects of GIPR antagonists alone and in combination with GLP-1R agonists in preclinical models. Science translational medicine *10*.

Laursen, T.L., Hagemann, C.A., Wei, C., Kazankov, K., Thomsen, K.L., Knop, F.K., and Gronbaek, H. (2019). Bariatric surgery in patients with non-alcoholic fatty liver disease - from pathophysiology to clinical effects. World journal of hepatology *11*, 138-149.

Lu, H., Howatt, D.A., Balakrishnan, A., Moorleghen, J.J., Rateri, D.L., Cassis, L.A., and Daugherty, A. (2015). Subcutaneous angiotensin II infusion using osmotic pumps induces aortic aneurysms in mice. J Vis Exp.

Lutz, T.A., and Bueter, M. (2016). The use of rat and mouse models in bariatric surgery experiments. Frontiers in nutrition *3*, 25.

Mah, A.T., Van Landeghem, L., Gavin, H.E., Magness, S.T., and Lund, P.K. (2014). Impact of diet-induced obesity on intestinal stem cells: hyperproliferation but impaired intrinsic function that requires insulin/IGF1. Endocrinology *155*, 3302-3314.

Mingrone, G., Panunzi, S., De Gaetano, A., Guidone, C., Iaconelli, A., Leccesi, L., Nanni, G., Pomp, A., Castagneto, M., Ghirlanda, G., et al. (2012). Bariatric surgery versus conventional medical therapy for type 2 diabetes. The New England journal of medicine *366*, 1577-1585.

Miyawaki, K., Yamada, Y., Ban, N., Ihara, Y., Tsukiyama, K., Zhou, H., Fujimoto, S., Oku, A., Tsuda, K., Toyokuni, S., et al. (2002). Inhibition of gastric inhibitory polypeptide signaling prevents obesity. Nature medicine *8*, 738-742.

Mootha, V.K., Lindgren, C.M., Eriksson, K.F., Subramanian, A., Sihag, S., Lehar, J., Puigserver, P., Carlsson, E., Ridderstrale, M., Laurila, E., et al. (2003). PGC-1 alpha-responsive genes involved in oxidative phosphorylation are coordinately downregulated in human diabetes. Nature genetics *34*, 267-273.

Nauck, M.A., Vardarli, I., Deacon, C.F., Holst, J.J., and Meier, J.J. (2011). Secretion of glucagon-like peptide-1 (GLP-1) in type 2 diabetes: what is up, what is down? Diabetologia *54*, 10-18.

Rao, J.N., and Wang, J.Y. (2010). Regulation of gastrointestinal mucosal growth. San Rafael (CA): Morgan & Claypool Life Sciences. .

Reimann, F., and Gribble, F.M. (2016). Mechanisms underlying glucose-dependent insulinotropic polypeptide and glucagon-like peptide-1 secretion. Journal of diabetes investigation *7 Suppl 1*, 13-19.

Rubino, F., Forgione, A., Cummings, D.E., Vix, M., Gnuli, D., Mingrone, G., Castagneto, M., and Marescaux, J. (2006). The mechanism of diabetes control after gastrointestinal bypass surgery reveals a role of the proximal small intestine in the pathophysiology of type 2 diabetes. Annals of surgery *244*, 741-749.

Rubino, F., Gagner, M., Gentileschi, P., Kini, S., Fukuyama, S., Feng, J., and Diamond, E. (2004). The early effect of the Roux-en-Y gastric bypass on hormones involved in body weight regulation and glucose metabolism. Annals of surgery *240*, 236-242.

Salehi, M., Prigeon, R.L., and D'Alessio, D.A. (2011). Gastric bypass surgery enhances glucagon-like peptide 1-stimulated postprandial insulin secretion in humans. Diabetes *60*, 2308-2314.

Salinari, S., Carr, R.D., Guidone, C., Bertuzzi, A., Cercone, S., Riccioni, M.E., Manto, A., Ghirlanda, G., and Mingrone, G. (2013). Nutrient infusion bypassing duodenum-jejunum improves insulin sensitivity in glucose-tolerant and diabetic obese subjects. American journal of physiology. Endocrinology and metabolism *305*, E59-66.

Sandoval, D. (2016). Roux-en-Y gastric bypass and vertical sleeve gastrectomy: divergent pathways to improved glucose homeostasis. Gastroenterology *150*, 309-312.

Sato, T., Vries, R.G., Snippert, H.J., van de Wetering, M., Barker, N., Stange, D.E., van Es, J.H., Abo, A., Kujala, P., Peters, P.J., et al. (2009). Single Lgr5 stem cells build crypt-villus structures in vitro without a mesenchymal niche. Nature *459*, 262-265.

Sparre-Ulrich, A.H., Gabe, M.N., Gasbjerg, L.S., Christiansen, C.B., Svendsen, B., Hartmann, B., Holst, J.J., and Rosenkilde, M.M. (2017). GIP(3-30)NH2 is a potent competitive antagonist of the GIP receptor and effectively inhibits GIP-mediated insulin, glucagon, and somatostatin release. Biochemical pharmacology *131*, 78-88.

Theodorakis, M.J., Carlson, O., Michopoulos, S., Doyle, M.E., Juhaszova, M., Petraki, K., and Egan, J.M. (2006). Human duodenal enteroendocrine cells: source of both incretin peptides, GLP-1 and GIP. American journal of physiology. Endocrinology and metabolism *290*, E550-559.

Theodorakis, M.J., Carlson, O., Muller, D.C., and Egan, J.M. (2004). Elevated plasma glucose-dependent insulinotropic polypeptide associates with hyperinsulinemia in impaired glucose tolerance. Diabetes care *27*, 1692-1698.

Tsakmaki, A., Fonseca Pedro, P., and Bewick, G.A. (2017). 3D intestinal organoids in metabolic research: virtual reality in a dish. Curr Opin Pharmacol *37*, 51-58.

Umeda, L.M., Silva, E.A., Carneiro, G., Arasaki, C.H., Geloneze, B., and Zanella, M.T. (2011). Early improvement in glycemic control after bariatric surgery and its relationships with insulin, GLP-1, and glucagon secretion in type 2 diabetic patients. Obesity surgery *21*, 896-901.

Verdam, F.J., Greve, J.W., Roosta, S., van Eijk, H., Bouvy, N., Buurman, W.A., and Rensen, S.S. (2011). Small intestinal alterations in severely obese hyperglycemic subjects. The Journal of clinical endocrinology and metabolism *96*, E379-383.

Wang, C., Zhu, C., Shao, L., Ye, J., Shen, Y., and Ren, Y. (2019). Role of Bile Acids in Dysbiosis and Treatment of Nonalcoholic Fatty Liver Disease. Mediators Inflamm *2019*, 7659509.

Zervos, E.E., Agle, S.C., Warren, A.J., Lang, C.G., Fitzgerald, T.L., Dar, M., Rotondo, M.F., and Pories, W.J. (2010). Amelioration of insulin requirement in patients undergoing duodenal bypass for reasons other than obesity implicates foregut factors in the pathophysiology of type II diabetes. Journal of the American College of Surgeons *210*, 564-572, 572-564.

Zhang, X., Young, R.L., Bound, M., Hu, S., Jones, K.L., Horowitz, M., Rayner, C.K., and Wu, T. (2019). Comparative effects of proximal and distal small intestinal glucose exposure on glycemia, incretin hormone secretion, and the incretin effect in health and type 2 diabetes. Diabetes care *42*, 520-528.

FIGURES

Figure 1

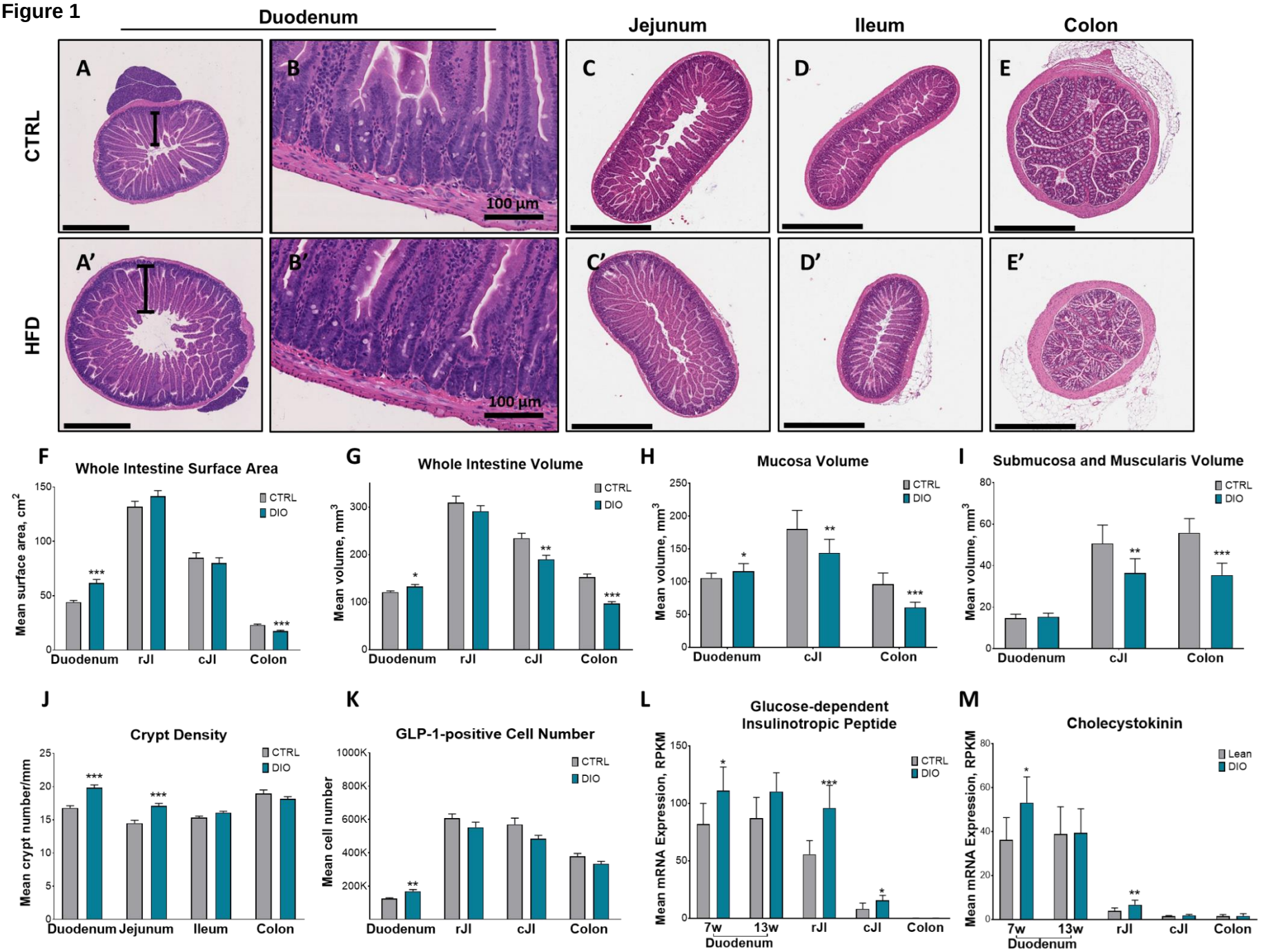
Duodenum
Jejunum
Ileum
Colon
CTRL
HFD
A
B
C
D
E
A'
B'
C'
D'
E'
100 µm
100 µm
F
Whole Intestine Surface Area
Mean surface area, cm2
CTRL
DIO
Duodenum
rJI
cJI
Colon
G
Whole Intestine Volume
Mean volume, mm3
H
Mucosa Volume
I
Submucosa and Muscularis Volume
J
Crypt Density
Mean crypt number/mm
Jejunum
Ileum
K
GLP-1-positive Cell Number
Mean cell number
L
Glucose-dependent Insulinotropic Peptide
Mean mRNA Expression, RPKM
7w
13w
M
Cholecystokinin
Lean

Figure 2

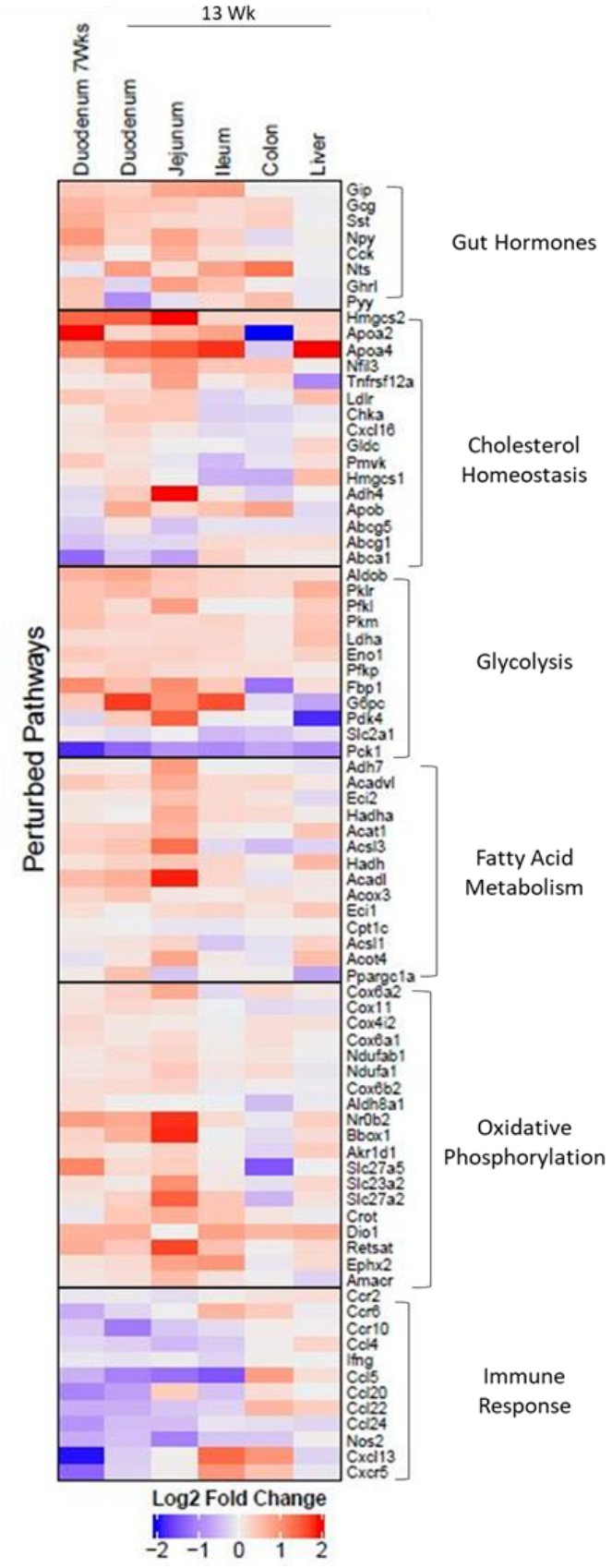
13 Wk
Duodenum 7Wks
Duodenum
Jejunum
Ileum
Colon
Liver
Perturbed Pathways
Gip
Gcg
Sst
Npy
Cck
Nts
Ghrl
Pyy
Gut Hormones
Hmgcs2
Apoa2
Apoa4
Nfil3
Tnfrsf12a
Ldlr
Chka
Cxcl16
Gldc
Pmvk
Hmgcs1
Adh4
Apob
Abcg5
Abcg1
Abca1
Cholesterol Homeostasis
Aldob
Pklr
Pfkl
Pkm
Ldha
Eno1
Pfkp
Fbp1
G6pc
Pdk4
Slc2a1
Pck1
Glycolysis
Adh7
Acadvl
Eci2
Hadha
Acat1
Acsl3
Hadh
Acadl
Acox3
Eci1
Cpt1c
Acsl1
Acot4
Ppargc1a
Fatty Acid Metabolism
Cox6a2
Cox11
Cox4i2
Cox6a1
Ndufab1
Ndufa1
Cox6b2
Aldh8a1
Nr0b2
Bbox1
Akr1d1
Slc27a5
Slc23a2
Slc27a2
Crot
Dio1
Retsat
Ephx2
Amacr
Oxidative Phosphorylation
Ccr2
Ccr6
Ccr10
Ccl4
Ifng
Ccl5
Ccl20
Ccl22
Ccl24
Nos2
Cxcl13
Cxcr5
Immune Response
Log2 Fold Change
−2 −1 0 1 2

Figure 3

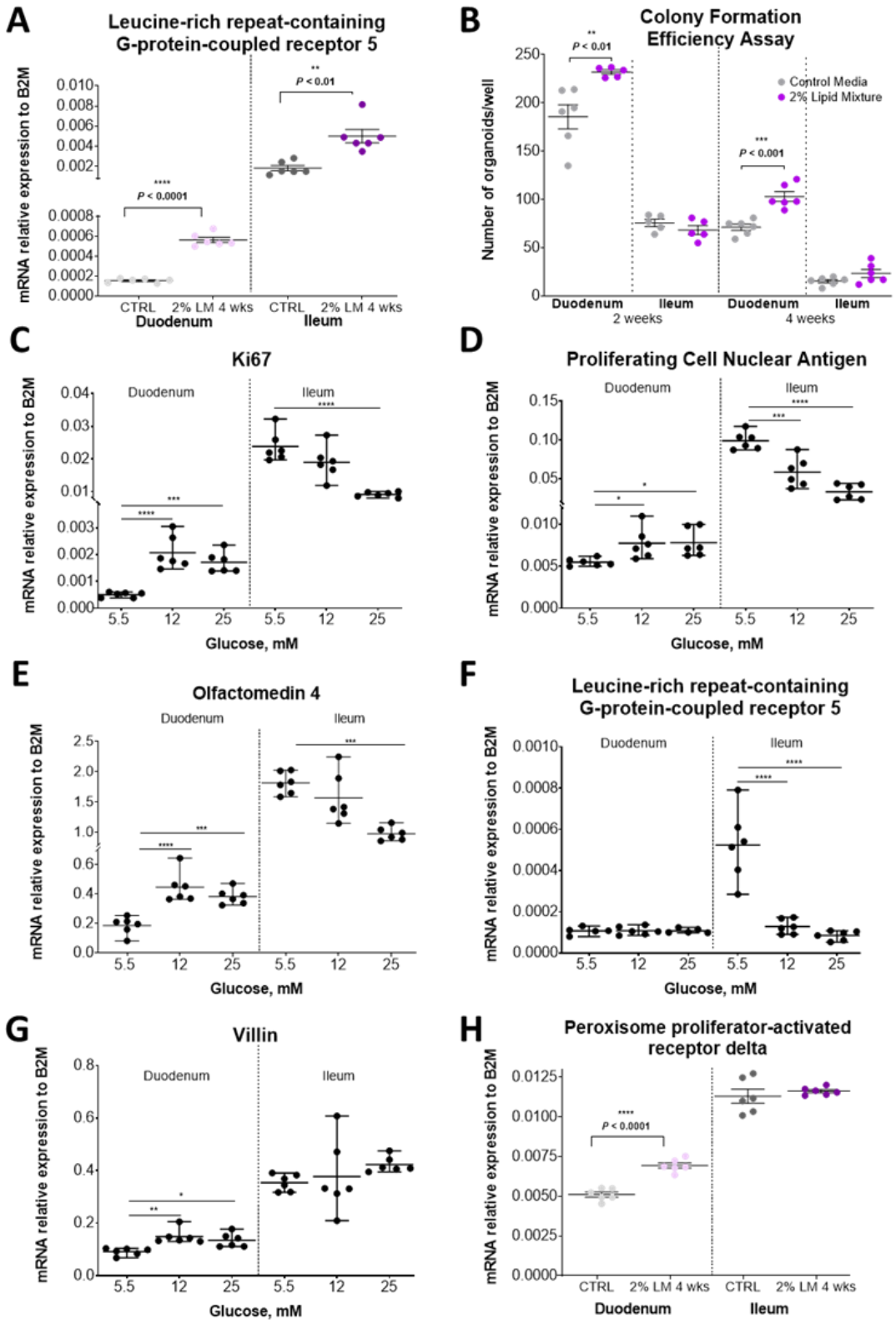
A
Leucine-rich repeat-containing G-protein-coupled receptor 5
mRNA relative expression to B2M
P < 0.0001
P < 0.01
CTRL
2% LM 4 wks
Duodenum
Ileum
B
Colony Formation Efficiency Assay
Number of organoids/well
Control Media
2% Lipid Mixture
P < 0.01
P < 0.001
Duodenum
Ileum
2 weeks
4 weeks
C
Ki67
D
Proliferating Cell Nuclear Antigen
E
Olfactomedin 4
F
Leucine-rich repeat-containing G-protein-coupled receptor 5
G
Villin
H
Peroxisome proliferator-activated receptor delta
Glucose, mM

Figure 4

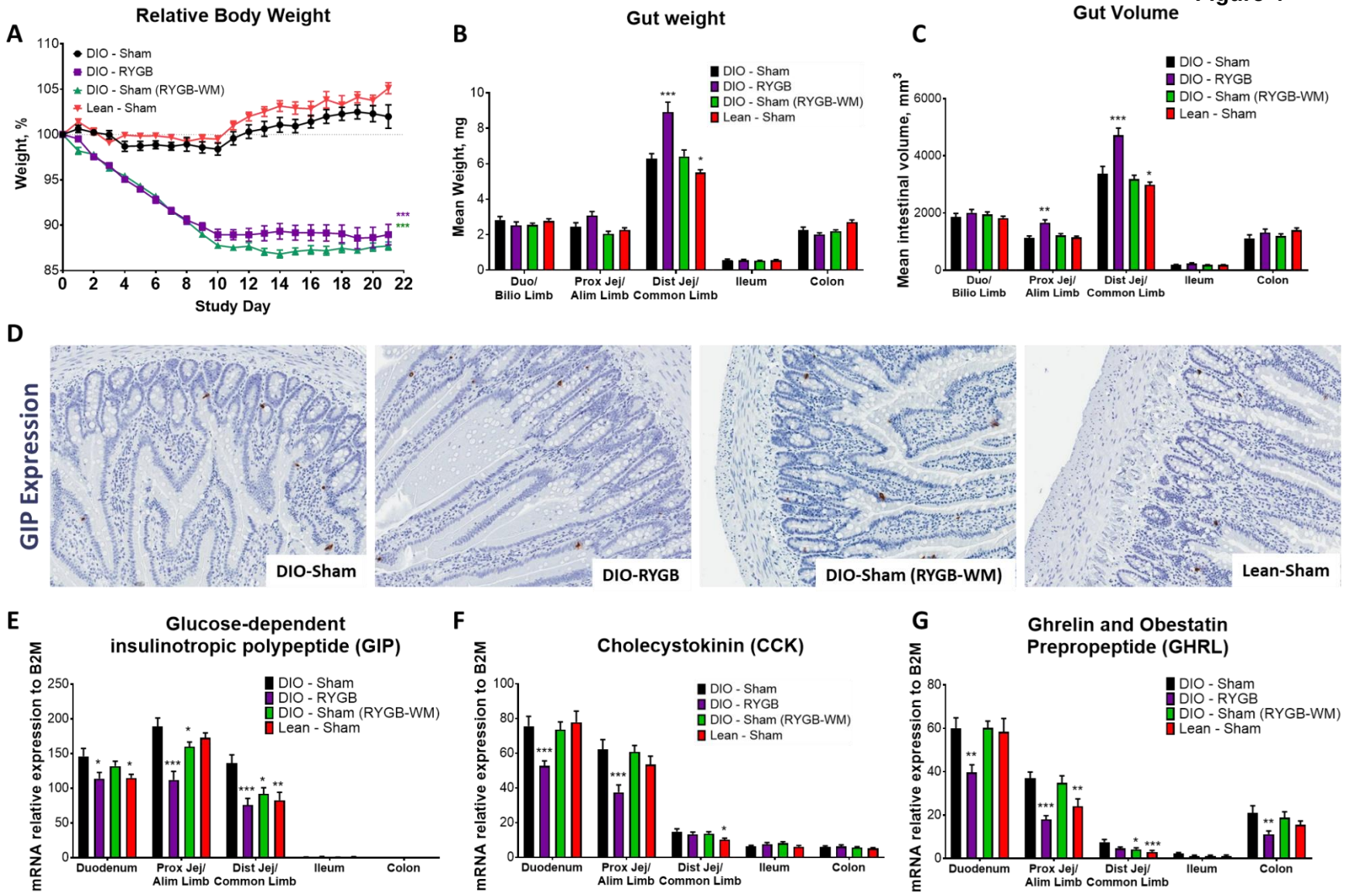
A
Relative Body Weight
DIO - Sham
DIO - RYGB
DIO - Sham (RYGB-WM)
Lean - Sham
Weight, %
Study Day
B
Gut weight
Mean Weight, mg
Duo/ Bilio Limb
Prox Jej/ Alim Limb
Dist Jej/ Common Limb
Ileum
Colon
C
Gut Volume
Mean intestinal volume, mm3
D
GIP Expression
DIO-Sham
DIO-RYGB
DIO-Sham (RYGB-WM)
Lean-Sham
E
Glucose-dependent insulinotropic polypeptide (GIP)
mRNA relative expression to B2M
F
Cholecystokinin (CCK)
G
Ghrelin and Obestatin Prepropeptide (GHRL)
Duodenum

Figure 5

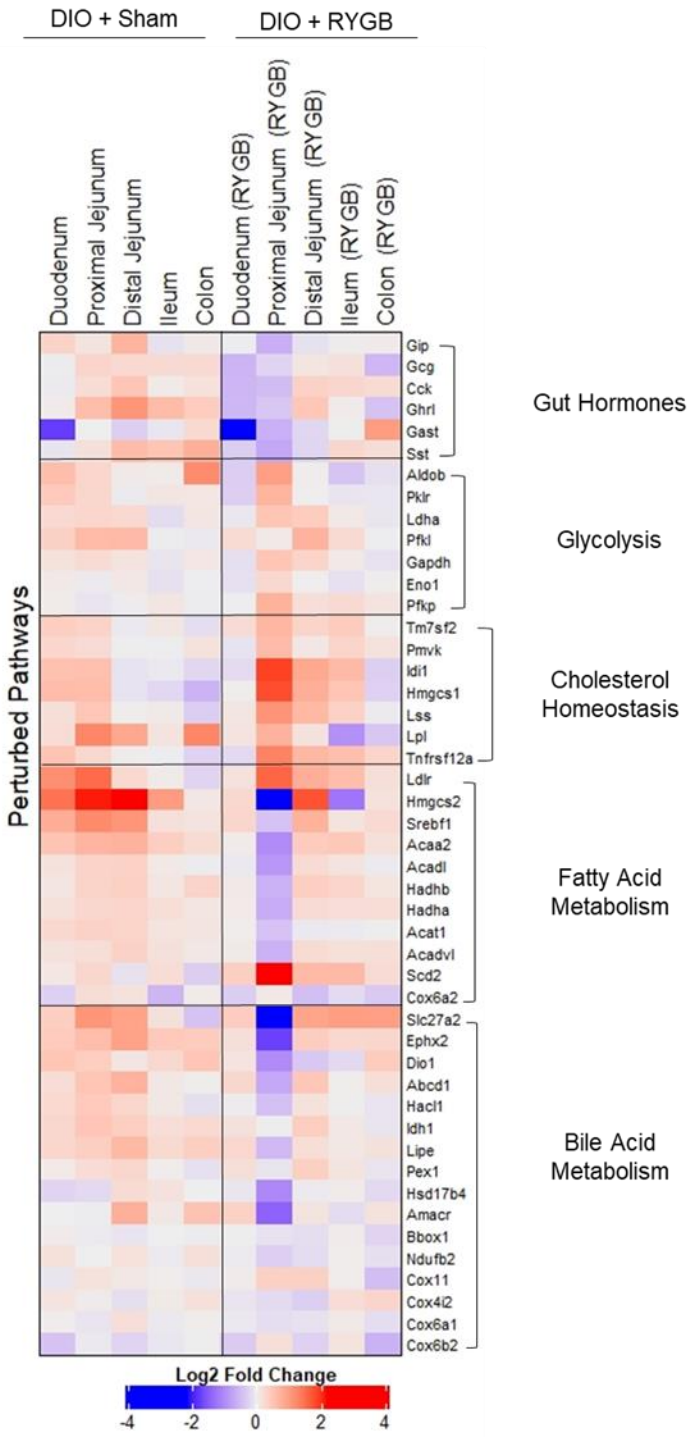
DIO + Sham
DIO + RYGB
Duodenum
Proximal Jejunum
Distal Jejunum
Ileum
Colon
Duodenum (RYGB)
Proximal Jejunum (RYGB)
Distal Jejunum (RYGB)
Ileum (RYGB)
Colon (RYGB)
Perturbed Pathways
Gip
Gcg
Cck
Ghrl
Gast
Sst
Gut Hormones
Aldob
Pklr
Ldha
Pfkl
Gapdh
Eno1
Pfkp
Glycolysis
Tm7sf2
Pmvk
Idi1
Hmgcs1
Lss
Lpl
Tnfrsf12a
Cholesterol Homeostasis
Ldlr
Hmgcs2
Srebf1
Acaa2
Acadl
Hadhb
Hadha
Acat1
Acadvl
Scd2
Cox6a2
Fatty Acid Metabolism
Slc27a2
Ephx2
Dio1
Abcd1
Hacl1
Idh1
Lipe
Pex1
Hsd17b4
Amacr
Bbox1
Ndufb2
Cox11
Cox4i2
Cox6a1
Cox6b2
Bile Acid Metabolism
Log2 Fold Change
-4
-2
0
2
4

Figure 6

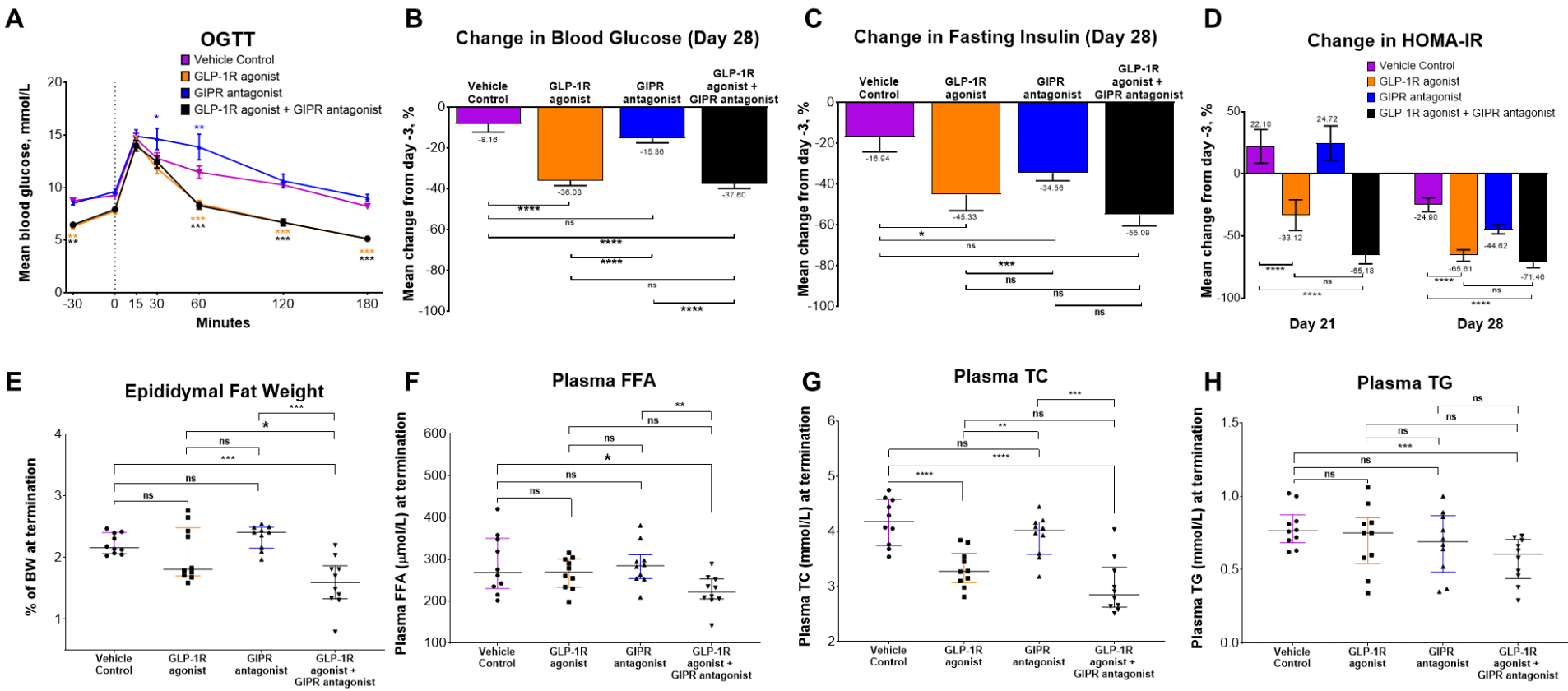
A
OGTT
Vehicle Control
GLP-1R agonist
GIPR antagonist
GLP-1R agonist + GIPR antagonist
Mean blood glucose, mmol/L
Minutes
B
Change in Blood Glucose (Day 28)
Mean change from day -3, %
-8.18
-36.08
-15.36
-37.60
C
Change in Fasting Insulin (Day 28)
Mean change from day -3, %
-16.94
-45.33
-34.56
-55.09
D
Change in HOMA-IR
Mean change from day -3, %
22.10
-33.12
24.72
-65.18
-24.90
-65.61
-44.62
-71.46
Day 21
Day 28
E
Epididymal Fat Weight
% of BW at termination
F
Plasma FFA
Plasma FFA (µmol/L) at termination
G
Plasma TC
Plasma TC (mmol/L) at termination
H
Plasma TG
Plasma TG (mmol/L) at termination
Vehicle Control
GLP-1R agonist
GIPR antagonist
GLP-1R agonist + GIPR antagonist

CONTEXT AND SIGNIFICANCE

Excessive consumption of unhealthy calories is a primary driver of insulin resistance and hyperinsulinemia underlying the obesity and metabolic disease epidemics. The gut regulates metabolism in health and disease. This paper reports that diet with high content of fat and/or sugar induces distinct and opposite effects in the growth and metabolism of the proximal vs distal gut; this morphologic and functional imbalance is associated with a dysmetabolic phenotype; and improved metabolic function after surgical and pharmacological intervention is associated with restored balance between proximal/distal intestine. These findings support the intestinal epithelium's role in metabolism control, suggesting interventions that maintain/restore physiological balance between the proximal and distal intestine may effectively prevent and treat T2D and other metabolic diseases (e.g., NAFLD/NASH, PCOS).

Word count: 120
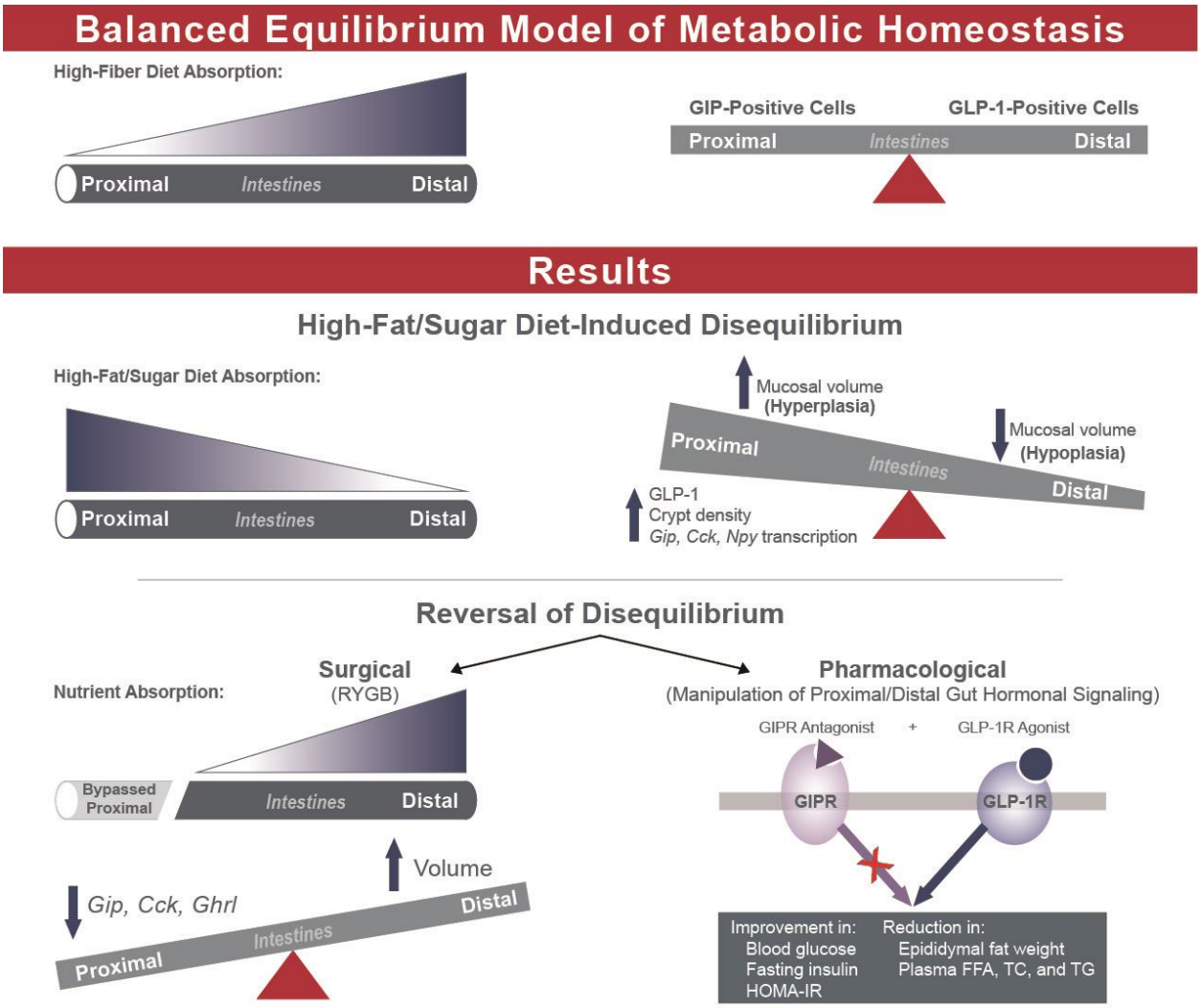
GRAPHICAL ABSTRACT